Conference Presentation

Ultrasonic sensor for UAV flight navigation

Davies, D.G, Bolam, R.C., Vagapov, Y., Excell, P.

This is a paper presented at the 25th Int. Workshop on Electric Drives: Optimization in Control of Electric Drives (IWED), Moscow, Russia, 31 Jan - 2 Feb 2018

Ultrasonic Sensor for UAV Flight Navigation

David Gareth Davies, Robert Cameron Bolam, Yuriy Vagapov, Peter Excell
School of Applied Science, Computing and Engineering,
Glyndwr University, Plas Coch, Mold Road,
Wrexham, LL11 2AW, UK

***Abstract*—Ultrasonic transducers were utilised for the design and development of an alternative method for flight instrumentation measurement of the velocity of unmanned air vehicles (UAVs). Current methods have been deemed to have significant shortcomings, such as the need for GPS thus leading to indoor UAV operations being incapable of velocity sensing. The proposed concept is developed from the utilisation of ultrasonic transit-time flowmeters. A test bench has been produced to measure the accuracy and confirm the validity of the concept. Two key design variables were determined – the optimal transducer mounting configuration and the optimal angle of incidence for the transducer mountings. The mounting configurations were analysed from common transit-time flowmeter sensor configurations and were tested using both CFD and acoustic simulations. The findings are presented and correlated based on these simulations and it was determined that a V-method configuration was the optimal choice. The correct angle of incidence was determined by an experimental methodology. The time-of-flight outputted from the transducers was compared to the calculated ideal value, and the findings revealed that an angle of 30° was the most accurate for the reflection of the emitted wave. The experimentation was conducted with a specially designed test bench and associated electronic hardware located in a wind tunnel. The test results have provided conclusive evidence that the overall design can produce accurate results comparable with current instrumentation sensors.**

Keywords—drone, UAS, unmanned air vehicle, ultrasonic guidance system, sensor technology, ultrasonic flight navigation

I. INTRODUCTION

The design and development of UAV technology is a new and a rapidly growing industry. This can be seen by the popularity it receives from both corporations and media alike. The UAV market is estimated to be $13.22 billion in 2016 and projected to reach $28.27 billion by 2020 [1]. This shows just how quickly this market is growing and how the technology is becoming an integral part of our society. New applications and innovations are constantly being implemented within the industry in a vast amount of sectors such as military use, hobby enthusiasts, and the agricultural industry.

As the applications and requirements of UAVs become more technologically advanced and operationally demanding, the systems that make up UAVs must equally evolve to step up to the task of fulfilling these requirements. Both engineers and researchers alike are constantly striving to continually design improvements within these systems. One such area of system design that is continually improved upon is UAV flight instrumentation. Flight instrumentation is a crucial area within the flight system, providing the end user with key data such as velocity, temperature, and humidity. This is also a significant contributor to a UAV's ability to provide automation in control. Current flight instrumentation systems present designers and engineers with many limitations some of which cannot be solved using current methods. These limitations include functions such as the inability to receive velocity and positioning data in areas where there is no GPS. Payload can also be an issue with current instrumentation as an increase in traditional sensors increases overall weight. The ability to utilise ultrasound into UAV flight instrumentation provides an innovative and exciting solution to many of these limitations.

The use of ultrasound in instrumentation is not a new concept. Current applications include medical uses and underwater navigation in the form of sonar. Another significant application is in the form of gas flowmeters. This application involves the ability of fluid intake to affect the measured velocity of a sound wave. Ultrasound in gas flowmeters has been a great success, with industrial experts claiming "in natural gas applications, ultrasonic flowmeters generally offer better performance, greater reliability, and lower capital and ownership costs than mechanical-type meters" [2]. By applying this same principle into UAV instrumentation, a range of potential opportunities in the field of UAV flight instrumentation is created. The research and development carried out in this report seeks to utilise these opportunities and produce an instrumentation system for UAVs that provides the industry with a sound, practical alternative to current instrumentation methods.

The most common method for UAV flight control and instrumentation is with inertial sensors in the form of inertial measurement units (IMUs). IMUs are a form of micro electro mechanical system (MEMS) and in their most basic form can be traced back as early as the 1970s [3]. In their most basic form, IMUs generally consist of an accelerometer and a rate gyro. The accelerometer is used to measure linear acceleration in three axes (a_x, a_y, a_z). The rate gyro is used to measure angular velocity relative to the body frame. This very basic form of IMU is rarely used as a stand-alone unit. In reality, IMUs often contain a number of additional sensors to create greater measurement accuracy and provide further data for the user [4]. This usually leads to increased cost for the user. Some possible additional sensors that are integrated into the IMU design include:

GPS: GPS receivers can provide measurements for heading, position, and velocity with respect to the inertial

978-1-5386-1200-2/18/$31.00 ©2018 IEEE

frame. These are very common on a wide range of IMUs from hobby usage to industrial and military applications. A major concern when using GPS sensors is loss of signal due to various reasons such as being inside a building. This can be problematic when being utilised on UAVs as a variety of UAV types such as camera hobby drones are often required to be used in a number of different environments. Another issue with using GPS receivers is that UAVs use central processing units (CPUs) with relatively low processing power. This is due to weight considerations and battery life saving. However, there is currently research into improving UAVs CPU processing power without compromising lightweight design.

Pressure sensors: Pressure sensors can be divided up into two main categories; relative pressure sensors and absolute pressure sensors. Relative pressure sensors can be used to measure air speed while absolute pressure sensors can be used to measure air pressure and thus estimate altitude. Pressure sensors in UAVs often utilise piezoresistive transducers [5] which are often subject to drift [6]. This is undesirable, as it means that over time pressure measurements will begin to drift away from accurate measurements, usually displaying Pascal readings much higher than the true data.

Anemometer: An anemometer acts as a three-axis wind velocity sensor i.e. velocity relative to the air around the sensor [7]. These can come in the form of sonic and mechanical anemometers. When being applied to UAVs, size can be problematic due to a decrease in accuracy as the sensor is decreased in size.

Although MEMS IMUs with additional sensors are the primary choice for most UAV commercial uses, there are other alternative technologies available. Vision-based guidance flight systems are offering an alternative approach to traditional IMUs, particularly in industrial applications. This can be seen through developments such as the COLIBRI helicopter [8]. This UAV integrates a vision based guidance system to minimise the use of GPS, although a GPS sensor is still integrated to assist with landing. Vision based guidance is also a popular choice for UAV space exploration, with GPS being unavailable. An example of integrated vision based guidance for UAV space exploration is the PERIGEO Project [9]. A key factor in this project is the inertial and imaging sensors that are integrated into the navigation system. Research has also been conducted into navigation systems that do not require gyros, offering a cost effective alternative to traditional IMUs. To determine attitude heading without the need for rate gyros, quaternion algorithms have been implemented that only require two non-linear vector measurements: gravitational field vectors and magnetic field vectors [10].

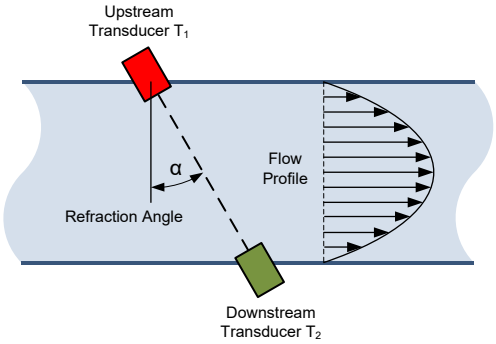

Fig. 1. The operating principle of a transit-time flow meter. An ultrasonic wave is emitted alternatively by both transducers, T_1 and T_2.

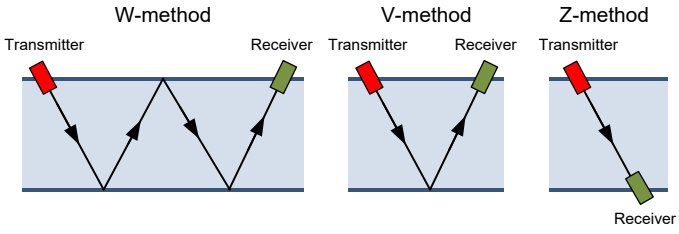

Fig. 2. The configurations of transit-time flow meter methods.

II. Ultrasonic Sensor

Applying ultrasonic wave propagation to act as an airflow velocity sensor is not a new concept. Ultrasonic flow meters are used in a number of applications amongst industries such as gas flow meters, hydraulic flow meters, and even in biomedical applications such as blood flow monitoring [11], [12]. In fact, the flow meter industry has estimated to be worth of $9.61 billion in 2021 [13].

There are two main types of flow meters – transit-time flow meters and Doppler flow meters. Which type to utilise in a flow meter design greatly depends on the fluid that will be travelling through. However, Doppler flow meters cannot be used for clean liquid with laminar flows, thus they are unsuitable for use in this project.

Transit-time flow meters act as an effective way to measure flow velocity in a clean fluid. Fig. 1 shows a diagram of the operating principles of transit-time flow meters. It can be seen that an ultrasonic signal is passed between two transducers, both upstream and downstream of the oncoming fluid. From the time taken for the signal to travel upstream and downstream, the flow velocity can be calculated using the following equation

$$v = \frac{D}{\sin 2\theta}\left(\frac{T_{up} - T_{down}}{T_{up} \times T_{down}}\right) \quad (1)$$

where D is the pipe diameter, θ is the angle of the emitted ultrasonic wave relative to the fluid flow, T_{up} is the time taken for the ultrasonic wave to travel upstream, and T_{down} is the time taken for the ultrasonic wave to travel downstream [14].

There are many different ways in which transducers are mounted. Although all the different mountings of the transducers rely on the same principles, these different configurations provide a change in the directional path of the emitted ultrasonic wave. These can prove advantageous depending on the flow meter's application. Within industry, there are generally three common methods employed for the mounting configurations of ultrasonic transducers. These are the V-method, Z-method, and W-method. These three methods are depicted as diagrams in Fig. 2.

All three methods have been investigated to accurately develop a methodology to analyse the sensor concept. This concept being the utilisation of ultrasonic transducers to act as a velocity output for UAVs.

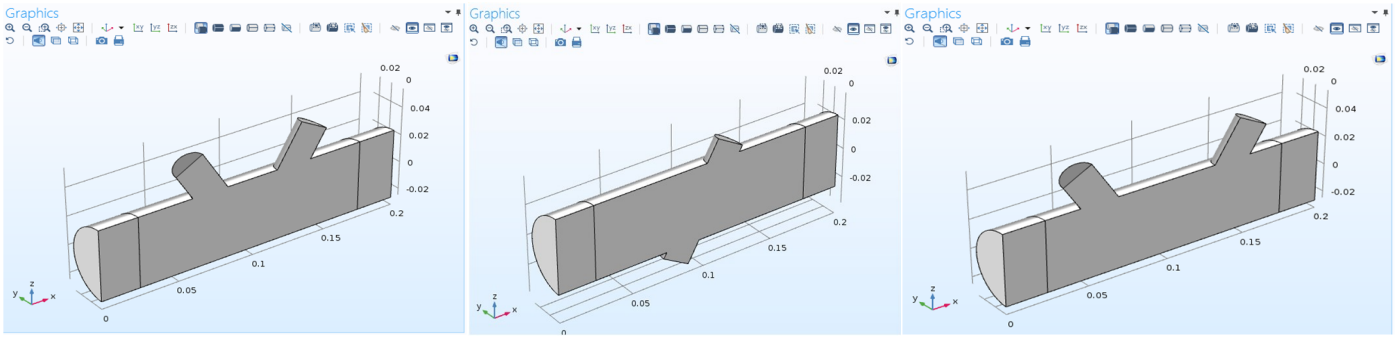

a) b) c)

Fig. 3. The final geometry for the method simulation: (a) V-method, (b) Z-method, (c) W-method.

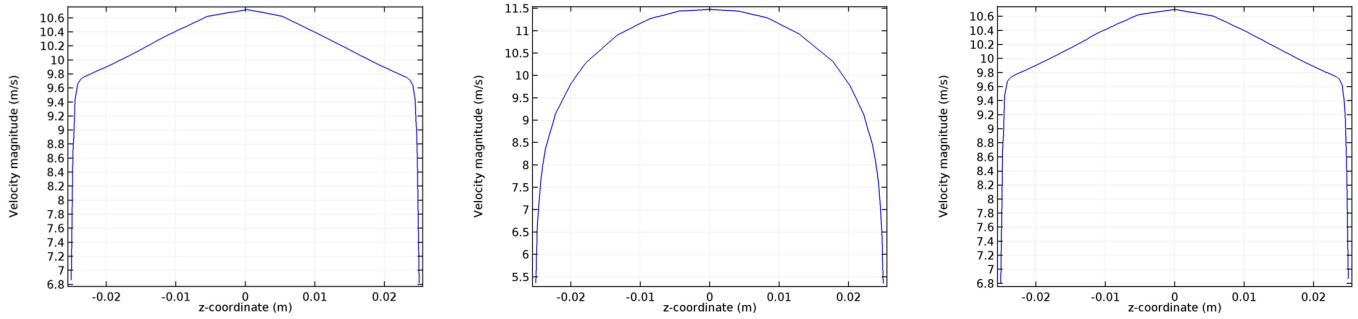

a) b) c)

Fig. 4. 1D plot graph of the average flow velocity along the z coordinate of the method configuration: (a) V-method; (b) Z-method; (c) W-method.

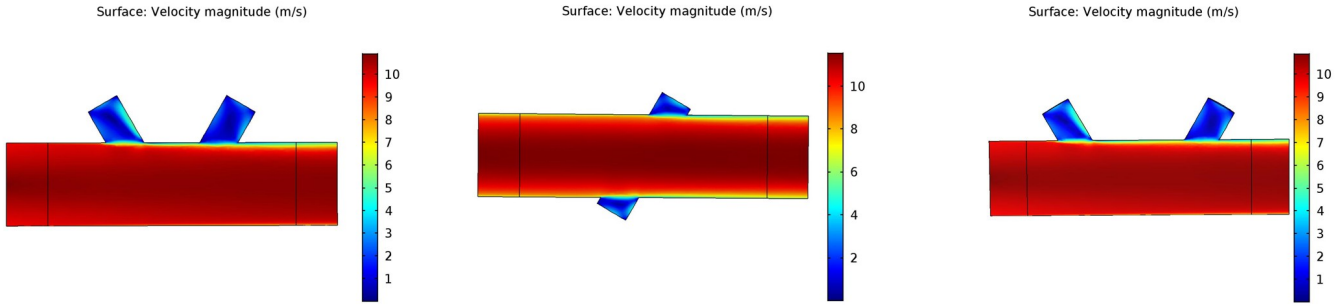

a) b) c)

Fig. 5. 3D graphic plot of flow velocity magnitude of the method configuration: (a) V-method; (b) Z-method; (c) W-method.

III. Sensor Modelling and Simulation

Two of the most crucial variables are the configuration in which the sensors are mounted within the flow meter and the angle of incidence at which the ultrasonic wave is emitted relative the fluid flow. This paper details the design procedures and methods used in the concept development: (1) determining the mounted sensor configurations through simulation, (2) determining the ultrasonic wave angle of incidence through experimentation.

It was determined that three mounting configurations would be modelled. The simulations were carried out using COMSOL Multiphysics 5.2 and consist of two stages – a CFD turbulence model simulation and a convected wave equation acoustic model simulation.

It was first necessary to create a working geometry and generate a mesh i.e. the computational domain generation. Fig. 3 shows the final geometries used in each of the three simulations. The geometries were created with a cylinder length of 200mm and a diameter of 50mm. This cylinder acted as a domain to represent the pipe of the test bench which would receive any incoming flow velocity. A further two cylinders (one cylinder for the Z-method configuration) were created to represent the ultrasonic transducers. A rotation function of 30° was applied to the transducer cylinders and the cylinder geometries were placed in such a way as to allow for the correct wave propagation travel between each transducer. The pipe cylinder and transducer cylinder were combined to create a single geometry domain using the form union function. The newly created single entity was then partitioned down the centre. This partition of the geometry was created by applying a work plane down the *z-x* plane of the geometry, then applying a partition object function and delete entities function respectively. To allow for a clear depiction of the ultrasonic wave propagation, the material applied to the geometry was water. This is due to the fact that the wave propagation will remain similar as if it was propagating through air, however the speed of sound in water is 1480m/s

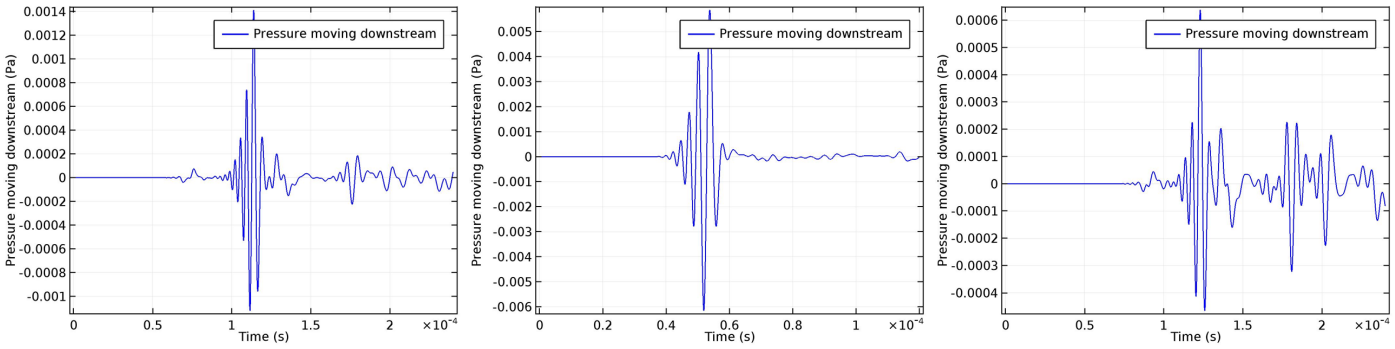

a) b) c)

Fig. 6. 1D plot graphs of the acoustic pressure signals at the receiving transducer over the simulated time period. (a) V-method; (b) Z-method; (c) W-method.

as opposed to 343m/s in air. This means that there will be less unwanted noise reflected before the emitted wave reaches the receiver. At this point, boundary definitions were made.

For all three configurations, the CFD mesh contained approximately 80,000 elements. It was important that the element sizing remained as uniform as possible, so as to ensure the same level of detail for the travelling wave propagation across the whole of the geometry. This was achieved by setting the minimum and maximum element size to similar figures. In all three configurations, the acoustic mesh yielded approximately 6000 elements.

There were two separate simulations carried out. First of all, the CFD simulations were conducted. This was necessary as the acoustic simulations contain inputted variables that rely on results obtained from the CFD simulation. The k-ε turbulence model was used. This model was selected as it has relatively low memory requirements. Also, the k-ε model is often used when there is very little or no curvature to the fluid flow. Boundary conditions were applied to the flow inlet, flow outlet, and boundary walls. The flow inlet was set at the left of the geometry and was set up with a 10m/s flow velocity, with boundary conditions of water. This modest flow velocity was chosen because it was necessary for the overall CFD simulation and it was not intended to determine how the ultrasonic waves would react to a large flow velocity.

Next, the acoustic simulations were conducted. A convected wave equation model was set up for the computational domain. For this model, variables required for setup were background mean flow velocity, pressure, temperature, and density. These variables were all obtained during the CFD simulation and were linked accordingly to the previous simulation results. Boundary conditions were applied to the various sections. The outside wall was set as a perfect acoustic impedance, to simulate the reflective waves following the initial emitted wave. As the pipe is open both at the inlet and outlet, it was important that both flow boundaries were set as absorbing layers. This allowed for any acoustic pressure to be completely absorbed by the boundary with no reflection. A wave velocity was set at the ultrasonic source to simulate the emitting ultrasonic transducer. The velocity was set using a frequency of 20MHz. The simulation solution was set to run over a period of 0.24ms with solutions computed at intervals of 33.3ns. Each configuration took approximately 1 hour 10 minutes to complete.

IV. Simulation Results

For all three sensor configurations, the background mean flow velocity 1D plot graph and 3D plot graphic are displayed. Fig. 4 displays the result plots of the average flow velocity for all three method configurations. Fig. 5 shows 3D graphic plots of flow velocity magnitude.

For all three sensor configurations, the acoustic pressure signal at the ultrasonic receiver 1D plot graph and the 3D graphic display of the acoustic signals wave propagation is displayed. The 3D acoustic wave propagation graphic for each sensor configuration is displayed three times – near the beginning of the simulation, near the middle of the simulation, and near the end of the simulation. Fig. 6 shows 1D plot graphs of the acoustic pressure signals at the receiving transducer over the simulated time period. Fig. 7, Fig. 8 and Fig. 9 display 3D graphics of the emitted acoustic wave.

The simulation results have been analysed in order to determine the optimum sensor mounting configuration. The first set of results reveal the findings of the mean flow velocity on a cross section of each of the three flowmeter configurations (Fig. 4 and Fig. 5). For the average flow velocity graph results are shown as z coordinates, thus starting at the lowest edge of the pipe then rising to the top of the pipe, where the transducers are positioned. Changes in the incoming air flow velocity will change the ultrasonic waves average velocity, thus reducing the accuracy of the velocity readings from the electronic hardware.

Fig. 4a and Fig. 5a related to the V-method show that the incoming flow velocity remains fairly evenly distributed from the bottom edge of the pipe to the top. It can be seen that within most of the pipe, the air flow velocity remains in the regions of approximately 9.7m/s and 10.6m/s. However, significant disturbances to the flow velocity can be seen to be created at the transmitter and receiver. This is due to both transducers being on the same edge of the flowmeter, thus creating a more uneven flow velocity between the top and bottom edge. These flow disturbances can be seen to create a flow velocity of, as low as, 3m/s. Due to only a thin layer of flow disturbance, this would have had little impact on the accuracy of the velocity sensing.

Fig. 4b and Fig. 5b show the average flow velocity and velocity magnitude of the Z-method configuration. It can be seen that through most of the pipe the velocity remains within

the region of 8.5m/s to 10.6m/s. From the average flow velocity across the *z*-axis graph, a much smoother transition between velocity changes can be seen. This is due to the sensors being on opposite sides of the flowmeter, thus creating an almost symmetrical flow velocity along the *z*-axis. It can be determined that the disturbances of the sensors have had almost no effect on the propagating wave, as the air flow velocity changes will allow for an evenly distributed wave propagation path. Fig. 4c and Fig. 5c display the average flow velocity and velocity magnitude of the W-method configuration. These results are almost identical to the V-method configuration, with both the transmitter and receiver being on one side causing significant disturbances and reductions in air flow velocity. Similar to the V-method configuration, these flow disturbances are unlikely to have a significant impact on the propagated wave velocity.

Fig. 6a shows a visualisation of the acoustic pressure of the emitted wave of the V-method configuration and a graph is plotted to show the received pressure throughout the simulation at the receiving transducer. From the 1D plot graph, the highest acoustic pressure difference can be seen as approximately 2.8mPa from peak to peak at approximately 115ms into the simulation. This is the intended desired signal from the receiver. Preceding this desired signal, very little disturbance can be seen. Following the desired signal however, significant pressure readings are picked up. This is undesirable, as this will create inaccuracies in the velocity output of the electronic hardware used in the final test bench. The magnitude of these undesirable waves following the intended acoustic signal can be seen as insignificant due to the magnitude of the pressure differential. This means that it will have a low impact on the accuracy of the electronic hardware. The analysis of the acoustic pressure graph is verified by the simulation graphics depicted in Fig. 7. The illustrations display the acoustic wave propagation at 30µs, 60µs, and 90µs thus showing the wave propagation at its starting and finishing positions with a mid-point also shown. By looking at the 60µs graphic, minor acoustic waves can be seen to have reached the

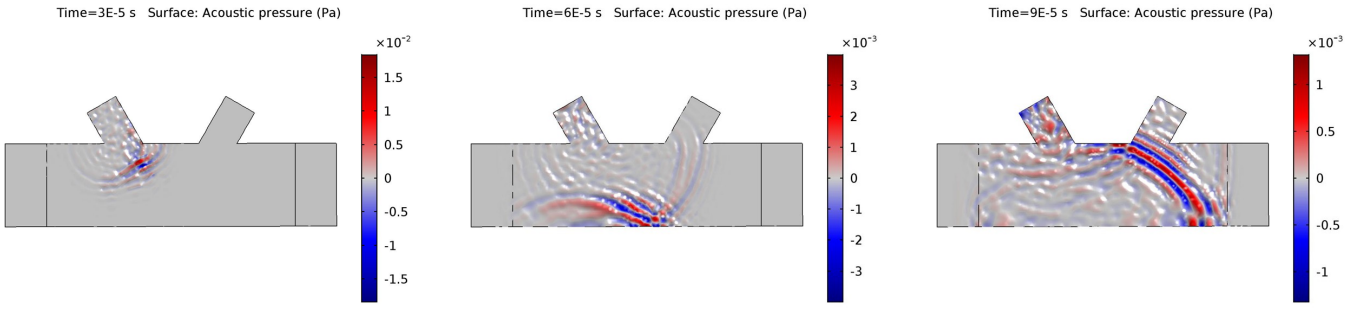

Fig. 7. 3D graphics of the emitted acoustic wave for the V-method configuration: (a) 30µs; (b) 60µs; (c) 90µs.

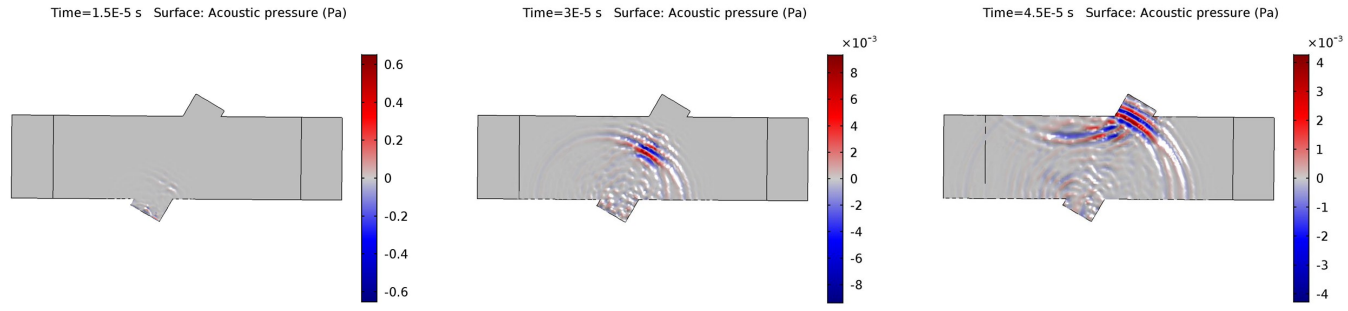

Fig. 8. 3D graphics of the emitted acoustic wave for the Z-method configuration: (a) 15µs; (b) 30µs; (c) 45µs.

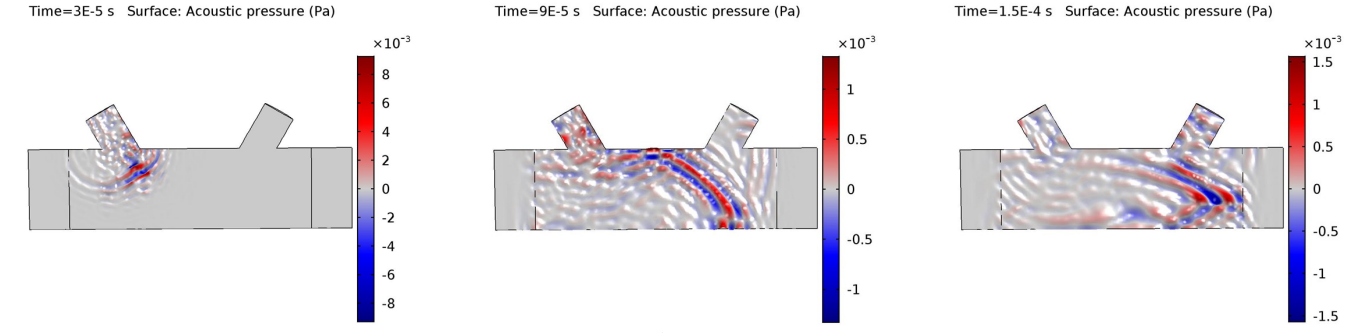

Fig. 9. 3D graphics of the emitted acoustic wave for the W-method configuration: (a) 30µs; (b) 90µs; (c) 150µs.

receiver before the intended signal. This is a verification of the small acoustic pressure difference seen at the initial stages of the acoustic pressure graph. On the 90µs graphic, the intended wave signal has reached the receiver. However, the wave has now increased in propagation, thus producing the undesirable acoustic signals following the intended wave that was seen in the acoustic pressure graph.

Fig 6b shows the results for the Z-method configuration simulation. The 1D plot graph shows that the intended ultrasonic signal pressure was approximately 18mPa peak to peak. This is preceded by almost no undesirable pressure differences, and succeeded by insignificant acoustic pressures. The illustrations in Fig. 8 provided for the Z-method configuration simulation are at 15µs, 30µs, and 45µs. This represents the start and finish point of the wave propagation, with a mid-point of acoustic signal. These illustrations verify the results seen in the acoustic pressure graph, with no disturbances seen before the wave has reached the receiver, and only minor undesired waves following the intended signal after it has reached the receiver.

Fig. 6c shows the results for the W-method configuration simulation. The 1D plot graph shows that the intended ultrasonic signal pressure was approximately 1.1mPa peak to peak. This intended signal is preceded by very little acoustic pressure differentials, however it is succeeded by very significant undesirable pressure differentials of magnitudes close to that of the intended acoustic signal. This is verified by the three illustrations (Fig. 9) of the W-method configuration which display illustrations of the simulation at 30µs, 90µs, and 150µs. At both the mid-point and final illustration, it can be seen that the wave has been significantly dissipated by the incoming air flow velocity, thus illustrating the undesirable signal readings discussed from the graph.

Based on the results discussed it was decided that the sensor mounting configuration for the final test bench should be the V-method. The results discussed of both the flow velocity magnitude and the accuracy of the received pressure signal both point to the Z-method configuration to be the optimal design configuration. However, in reality, this sensor would be miniaturised by using customised, specifically designed transducers. As the requirement of miniaturisation would be of priority for the mass manufacturing, the need for accuracy within the sensor becomes ever increasingly important. Due to a major effect on the accuracy of the overall

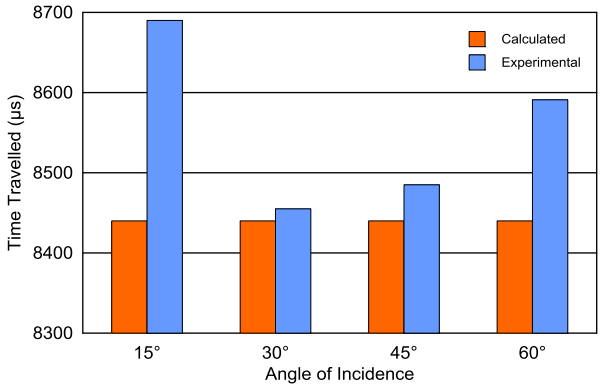

Fig. 10. Comparison between the four tested angles of incidence against the ideal calculated value.

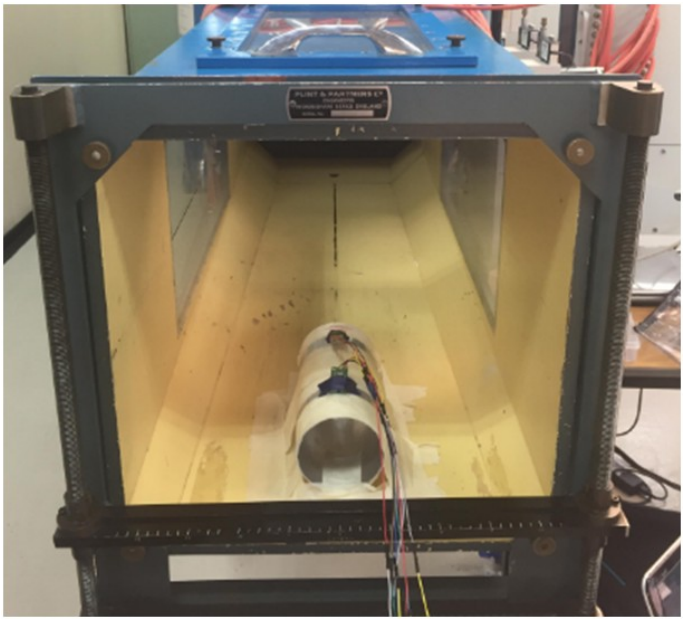

Fig. 11. The final test bench set up for experimentation within the low speed wind tunnel.

sensor being the total distance travelled, it cannot be deemed feasible to develop a miniaturised sensor that could cater to a Z-method transducer configuration. At least one point of reflection is needed. As for the W-method configuration, it can be seen that the W-method wave signals are highly propagated by the time they have reached the receiving transducer, thus rendering them far too inaccurate. Therefore, the V-method provides an excellent compromise between accuracy of the signal and the total distance travelled by the ultrasonic wave.

V. Sensor Angle of Incidence

Analysis of the sensor angle of incidence was based on the experimental results. The test reading obtained from the experiment were compared against the ideal value. The ideal value was calculated by measuring the distance between each transducer which was 494mm. By then taking the speed of sound to be 343m/s resulted in a calculated ideal time travelled by the signal of 1440µs. A delay of 7ms was set between the transducers, meaning the total ideal time being used as a comparison on each graph is 8440µs. Fig. 10 displays a graph comparing all 4 angles of incidence. These values were calculated by taking an average of the 10 readings for each angle. It shows a comparison of the averaged results for all angles of incidence against the ideal calculated value. It is clear to see that the most accurate angle of incidence was 30°, thus it was selected as the angle of incidence for the final experimental test bench.

VI. Results of the Experiment

Once both the sensor mounting configuration and the angle of incidence for the sensor had been determined, experimentation for the final design of the test bench with the electronic hardware was conducted. This experiment utilised the low speed wind tunnel (Fig. 11) to determine the accuracy and validity of the design concept.

When designing the electronic instrumentation hardware, choosing the right ultrasonic transducers was crucial. A number of ultrasonic transducers were analysed, and it was decided that the most suitable transducers for the experiment were the SRF235 Ultrasonic Rangers. These transducers are designed to emit an ultrasonic beam of just 15° and a minimum accurate distance reading of 100mm due to a relatively high frequency of 235kHz [15]. Also, these transducers use an I2C bus system, thus allowing a simpler circuit to be designed as a result of each transducer running through the same IO pins with separate bus addresses. This is beneficial due to the requirement of a small test bench.

For the implementation and controlling of the hardware, an Arduino Uno R3 board was used. An LCD05 display was used to display the required outputs of time taken for each emitted ultrasound wave to travel. This display was selected because, like the SRF235 Ultrasonic Rangers, it has the ability to be implemented using an I2C bus system.

The electronic hardware was activated while the transducers were in the test bench to ensure a zero velocity reading. Once this zero reading was given the wind tunnel was turned on, with speeds of 0m/s to 30m/s in intervals of 5m/s. For each interval of 5m/s, 10 readings were taken from the electronic hardware which could then be compared to the speed set on the wind tunnel.

The most significant variable that had an impact on the results was the oncoming air flow velocity and at the higher wind tunnel velocities greater discrepancies can be seen. This is due to the relatively low acoustic pressures emitted by the SRF235 ultrasonic transducers. Due to the low acoustic intensity, higher oncoming air flow velocities carry the emitted wave back to the emitting transducer as opposed to reaching the receiving transducer on upstream readings. This suggests that much higher frequency receivers should be used with greater acoustic intensity. Based on this analysis the bar chart displaying the averaged velocity readings, for each of the wind tunnel speeds in Fig. 12, only takes into account the first three readings at each speed.

V. Conclusion

The ultrasonic sensor concept, to provide an accurate method of velocity sensing in UAV flight instrumentation, has been validated through the use of numerical, experimental, and simulated methods. The CFD and acoustic simulations carried out have conclusively identified that the most effective sensor mounting configuration for the design is a V-method configuration. The experimentation that took place to determine the correct angle of incidence at which to reflect the emitted ultrasonic wave has concluded that the optimum angle to use for the test bench was 30°. The final experimentation, using the test bench and electronic hardware, has provided conclusions for the overall design and shown that it can produce accurate results which compare with those of current instrumentation sensors. Future work in this field is envisaged in the miniaturisation of the equipment, facilitating its installation on UAVs, with orthogonally arranged transducers for the determination of navigational velocity vector data.

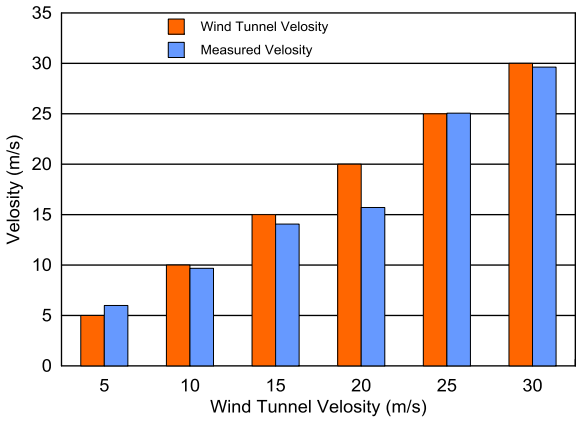

Fig. 12. An average of the first 3 readings of the each of the measured velocities compared to the wind tunnel test velocities.

References

[1] MarketsAndMarkets. (2017, 27 May). UAV market worth 28.27 billion USD by 2020 [Online]. Available: http://www.marketsandmarkets.com/PressReleases/unmanned-aerial-vehicles-uav.asp

[2] M. Bragg, "How ultrasonic flow meters measure natural gas more efficiently," *Flow Control*, vol. 21, no. 3, pp. 22-26, March 2015.

[3] R.L. Greenspan, "Inertial navigation technology from 1970 – 1995," *NAVIGATION: Journal of The Institute of Navigation*, vol. 42, no. 1, pp. 165–185, 1995.

[4] H. Chao, C. Coopmans, L. Di, and Y. Chen, "A comparative evaluation of low-cost IMUs for Unmanned Autonomous Systems," in *Proc. IEEE Int. Conf. on Multisensor Fusion and Integration for Intelligent Systems*, Salt Lake City, UT, USA, 5-7 Sept. 2010, pp. 211-216.

[5] R.H. Czichy, "Aerospace sensors," in *Sensors: Micro- and Nanosensor Technology-Trends in Sensor Markets*, vol. 8, H. Meixner, and R. Jones, Eds. Weinheim: VCH, 1995, pp. 365–411.

[6] E. Tolman, "Identifying pressure sensor problems," *Flow Control*, vol. 18, no. 7, pp. 22-26, July 2012.

[7] D. Zachariah, and M. Jansson, "Self-motion and wind velocity estimation for small-scale UAVs," in *Proc. IEEE Int. Conf. on Robotics and Automation, Shanghai*, China, 9-13 May 2011, pp. 1166-1171.

[8] L. Mejias, J.F. Correa, I. Mondragon, and P. Campoy, "COLIBRI: A vision-guided UAV for surveillance and visual inspection,' in *Proc. IEEE Int. Conf. on Robotics and Automation*, Rome, Italy, 10-14 April 2007, pp. 2760-2761.

[9] P. Molina, E. Angelats, I. Colomina, A. Latorre, J. Montano, and M. Wis, "The PERIGEO project: Inertial and imaging sensors processing, integration and validation on UAV platforms for space navigation," in *Proc. European Calibration and Orientation Workshop*, Castelldefels, Spain, 12-14 February 2014, pp. 79-85.

[10] D. Gebre-Egziabher, G.H. Elkaim, J.D. Powell, and B.W. Parkinson, "A gyro-free quaternion-based attitude determination system suitable for implementation using low cost sensors," in *Proc. IEEE Position Location and Navigation Symp.*, San Diego, CA, USA, 13-16 March 2000, pp. 185-192.

[11] D. Zheng, J. Mei, and M. Wang, "Improvement of gas ultrasonic flowmeter measurement non-linearity based on ray tracing method," *IET Science, Measurement & Technology*, vol. 10, no. 6, pp. 602-606, 2016.

[12] M. Nitzan, "Automatic noninvasive measurement of arterial blood pressure," *IEEE Instrumentation and Measurement Magazine*, vol. 14, no. 1, pp. 32-37, Feb. 2011.

[13] Flow Control Staff, "Petrochemicals and refining industries boost global demand for flowmeters," *Flow Control*, vol. 22, no. 7, p. 6, July 2016.

[14] Theultrasonicflowmeters.com. (2012, 15 Dec). Ultrasonic flow measurement technology [Online]. Available: http://www.theultrasonicflowmeters.com/flowmeas-transittime.htm

[15] Robot Electronics. (2015, 28 Oct). SRF235 Ultrasonic range finder. Technical specification [Online]. Available: https://www.robot-electronics.co.uk/htm/srf235tech.htm